Journal of Neurochemistry

JOURNAL OF NEUROCHEMISTRY | 2014 | 128 | 431–444 doi: 10.1111/jnc.12458

ORIGINAL ARTICLE

Changes in CNS cells in Hyperammonemic portal hypertensive rats

Silvina Tallis,*,† Laura R. Caltana,‡ Pablo A. Souto,*,† Amalia E. Delfante,*,† Néstor R. Lago,† Alicia Brusco‡ and Juan C. Perazzo*,†

*Laboratory of Hepatic Encephalopathy and Portal Hypertension, Faculty of Pharmacy and Biochemistry, University of Buenos Aires, Buenos Aires, Argentina

†Laboratory of Experimental Pathology, Faculty of Medicine, University of Buenos Aires, Buenos Aires, Argentina

‡Institute of Cell Biology and Neuroscience, Faculty of Medicine, University of Buenos Aires, Buenos Aires, Argentina

Abstract

Rats with pre-hepatic portal hypertension because of partial portal vein ligation develop minimal hepatic encephalopathy (MHE) with hyperammonemia, impaired blood–brain barrier, mild brain edema, and severe mitochondrial changes in the hippocampus. The aim of this study was to evaluate changes of different neural cells in the cerebral cortex and the hippocampus. Animals were divided into two groups, MHE and sham. Astrocytes were studied by immunostaining with glial fibrillary acidic protein and S100β protein; neurons were immunostained with neuronal nuclear marker, microtubule associated protein-2, and NF-200 and capillaries with Nestin. The hypoxia-inducible factor 1α (HIF-1α) and its downstream proteins, P-glycoprotein (P-gp) and erythropoietin receptor (Epo-R), were also evaluated. Astrocytes were increased in area and number only in the hippocampus, while S100β increased in both brain areas in MHE animals. Microtubule associated protein-2 and NF-200 immunoreactivities (-ir) were significantly reduced in both areas. Hippocampal Nestin-ir was increased in MHE animals. These cellular changes were similar to those described in ischemic conditions, thus HIF-1α, P-gp, and Epo-R were also evaluated. A high expression of HIF-1α in cortical neurons was observed in the MHE group. It is likely that this hypoxia-like state is triggered via ammonia occupying the binding domain of HIF-1α and thereby preventing its degradation and inducing its stabilization, leading to the over-expression of P-gp and the Epo-R.

Keywords: ammonia, hypoxia, minimal hepatic encephalopathy.

J. Neurochem. (2014) **128**, 431–444.

In hepatic disease, hepatocellular dysfunction results in impaired clearance of ammonium by the liver resulting in an altered ammonium homeostasis and interorgan trafficking of ammonia (Olde Damink *et al.* 2002). Patients with liver disease may develop splanchnic hyperdynamic syndrome, portal hypertension, collateral veins that divert portal blood with high ammonium content to the systemic circulation. Both, the incomplete clearance of ammonium and the development of collateral portal circulation contribute to hyperammonemia generally present in liver failure.

One of the most severe complications of acute or chronic liver failure is hepatic encephalopathy (HE) and ammonia appears as a key factor in the pathogenesis. Astrocyte swelling is the neuropathological characteristic change in acute HE. The histopathological hallmark in chronic liver failure was described by Norenberg (Norenberg 1977) consisting in the so-called Alzheimer type II astrocytes, described in both humans and experimental models of advanced HE.

Received June 26, 2013; revised manuscript received September 14, 2013; accepted September 16, 2013.

Address correspondence and reprint requests to Silvina Tallis, Uriburu 950 5°. Centro de Patología Experimental. Universidad de Buenos Aires. Facultad de Medicina. Ciudad Autónoma de Buenos Aires (1114). Buenos Aires. Argentina. E-mail: stallis@ffyb.uba.ar

Abbreviations used: Ca^{2+}, calcium; CLF, chronic liver failure; CNS, central nervous system; Cx, cortex; Epo-R, erythropoietin receptor; GFAP, glial fibrillary acidic protein; HE, hepatic encephalopathy; HIF 1-α, hypoxia inducible factor -1α; -ir, -immunoreactivity; MAP-2, microtubule associated protein-2; MHE, minimal hepatic encephalopathy; NeuN, neuronal nuclear marker; Nf-200, neuronal filaments 200 kDa; P-pg, P-glycoprotein; PVL, portal vein ligation.

We have previously showed that rats with pre-hepatic portal hypertension because of partial portal vein ligation (PVL) develop minimal hepatic encephalopathy (MHE) with morphological and functional changes in the CNS. Besides this, mitochondrial damage in hippocampus and in the integrity of the blood–brain barrier (Lores-Arnaiz *et al.* 2005 and Eizayaga *et al.* 2006) is also observed in this experimental model. More recently, we reported the presence of apoptosis in hippocampus in the same experimental model (Bustamante *et al.* 2011). The International Society for the Study of Hepatic Encephalopathy and Nitrogen metabolism (ISHEN) guidelines for experimental hepatic encephalopathy experimental models published that graded PVL can be regarded as a valid model of MHE (Butterworth *et al.* 2009).

The aim of this study was to evaluate morphological and functional cellular changes in two areas closely interrelated to cognitive abilities of the CNS in an experimental model of MHE induced by graded PVL (Vorobioff *et al.* 1983 and Abraldes *et al.* 2006). From this morphofunctional view, the two selected areas were the cortical layer V of the lateral parietal association cortex (Cx) and hippocampal CA1.

Material and methods

Animals

Fifty-eight male adult Wistar Kyoto rats (250–280 g), from the Animal Facility of the School of Pharmacy and Biochemistry, University of Buenos Aires, were used. Animal handling was in accordance with the American Physiological Society 'Guiding Principles in the Care and Use of Animals' and with the 6344/96 regulation of Argentine National Drug, Food and Medical Technology Administration (ANMAT). The study was in compliance with the ARRIVE guidelines.

Partial portal vein ligation

Rats were divided at random into two groups (n = 29), MHE and sham. PVL model was induced by performing a graded stenosis of the portal vein (Vorobioff *et al.* 1983). Briefly, rats were anesthetized with ether; a midline abdominal incision was made, a 20-gauge blunt-end needle was placed alongside the portal vein, and a 3-0 silk ligature was placed around the vein and snugly tied. The needle was subsequently removed to yield a calibrated stenosis of the portal vein. Sham-operated rats underwent identical surgical procedure except for the portal vein which was exposed and narrowed but not stenosed; it means that sham animals were treated identically in every respect, except for the permanent stricture.

Portal pressure, arterial blood pressure, plasma ammonia determination, and biochemical parameters

Ten days after portal vein stenosis, a pool of five rats of each group was anesthetized with sodium pentobarbital (40 mg/Kg, i.p). To measure portal pressure, a midline abdominal incision was made, the spleen exposed and a needle placed in the splenic pulp, fixed with cyanoacrilate glue, and connected to a pressure transducer through a polyethylene cannula (PE 50) filled with heparinized saline solution (25 U/mL). The needle was connected to a Statham Gould P23ID pressure transducer (Statham, Hato Rey, Puerto Rico) coupled to a Grass 79D polygraph (Grass Instrument, Quincy, MA, USA) for the measurement of portal pressure.

Twenty-four and forty-eight hours after surgery (over the first two post-operative days), a pool of five rats of each group was used for the measurement of arterial blood pressure using the SC1000 Blood Pressure Analysis System (Hatteras Instruments, Cary, NC, USA) and arterial blood parameters were determined using the Cobas soft (USA).

Ten days after surgery, a pool of five rats of each group was used for the determination of ammonia and for arterial blood parameters. Plasma ammonia concentrations were determined using 'Ammoniac Enzymatique U.V. kits', Biomerieux (France).

Fixation and tissue processing

After 10 days of surgery, ten rats of each group were anesthetized and fixed by perfusion according to Evrard *et al.* (2006).

Another set of animals, four rats of each group, were killed and brains were removed and fixed by immersion. Hematoxylin & Eosin stained was performed, to search for astrocytes Alzheimer type II.

Immunohistochemistry

Immunohistochemistry was performed as described previously (Evrard *et al.* 2006) with primary antibodies to glial fibrillary acidic protein (GFAP) (1 : 3000); S-100β protein (1 : 800); nuclear neuronal marker (NeuN) (1 : 1000); microtubule-associated protein-2 (MAP-2) (1 : 1000); neuronal filament 200 kDa (Nf-200) (1 : 1000); and Nestin (1 : 600). For the study of the hypoxic state, hypoxia-inducible factor 1α (HIF 1α) (1 : 1000); P-glycoprotein (P-gp) (1 : 500); and erythropoietin receptor (Epo-R) (1 : 500) were used. For immunofluorescent labeling, after incubating primary antibodies, brain sections were incubated with Fluorescent Fab2 anti-mouse and anti-rabbit secondary antibodies (1 : 500) (Caltana *et al.* 2009).

Morphometric digital image analysis

To ensure objectivity, for each set of experiments, all measurements were performed on coded slides, in blind conditions, by three observers (ST, LRC, and NRL). Measurements of both groups of control and treated sections were carried out in standardized conditions (at the same session, in the same day, by the same observer). In each tissue section, each microscopic field was selected within the limits of each anatomical area of interest to be morphometrically analyzed.

Tissue images were acquired on Axiolab Zeiss epifluorescence microscope equipped with a CCD camera QColor3, Olympus (Tokyo, Japan). Morphometric parameters of GFAP immunoreactive astrocytes, MAP-2 and Nf-200 immunoreactive neurons, Nestin stained vessels, cell counts, and mean gray level of S100-β immunostained astroglial cells were performed using the NIH Image J software (NIH, Bethesda, MD, USA). Plates were made with Adobe Photoshop 7.0 software (Adobe Systems Inc, San Jose, CA, USA).

For the GFAP- immunoreactivity (-ir), the cell area was evaluated. It was measured by interactively determining each cell limit. For Nestin-ir, the vessel area was evaluated, which is measured by determining each limit. To evaluate the MAP-2-ir and Nf-200-ir fibers, the total area of the immunolabeled fibers was related to the total area of the corresponding microscopic field, thus rendering a relative area parameter. For GFAP positive astrocytes and NeuN positive neurons, cell counting was represented by the

number of cells per microscopic field. The intensity of the S-100β immunoreactivity was evaluated by means of a relative optical density value (Ramos *et al.* 2000).

Statistical analysis

Reported values in tables and figures are mean values ± SEM. For the immunohistochemical analysis, individual experiments were composed of six to ten tissue sections of each animal from each group. Five to ten fields were measured from each brain area in each section of each animal. Reported values represent the mean ± SEM of experiments performed for each marker and each brain area. Differences among the means of the two groups were compared using an unpaired Student's *t*-test. When significant differences were detected, a two-tailed Student's *t*-test was performed for each pair of results. Statistical significance was set to $p < 0.05$. For the statistical analysis, GraphPad Prism v3.00 software (GraphPad Software Inc., San Diego, CA, USA) was used.

Results

Determination of portal pressure and plasma ammonia concentrations

Portal blood pressure was significantly increased in the MHE group (12.0 ± 0.4 mmHg) after 10 days of PVL as compared with the sham group (8.5 ± 0.2 mmHg); $p < 0.0001$. Similarly, plasma ammonia concentration in MHE rats was 2.9 times increased being 41.28 ± 1.751 μM as compared with the sham group, 14.24 ± 0.472 μM; $p < 0.0001$.

Presence of Alzheimer type II astrocytes

The hallmark of HE, Alzheimer type II astrocytes, was specially searched in the Cx and hippocampal areas; they were present neighboring the pyramidal layer of the hippocampus (Fig. 1).

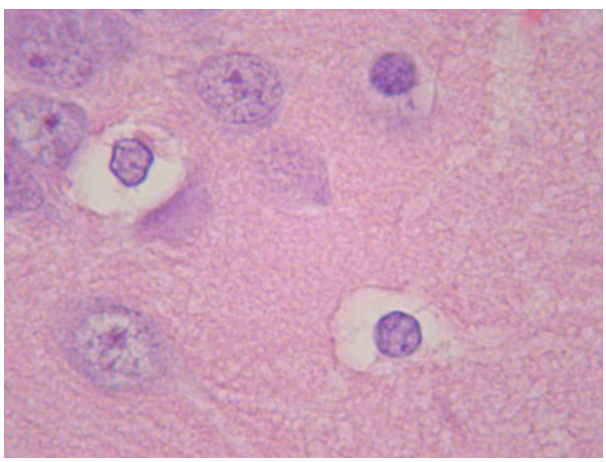

Fig. 1 Pyramidal layer of the hippocampus of minimal hepatic encephalopathy (MHE) animals showing the presence of Alzheimer type II astrocytes. Hematoxilin & Eosin, original magnification ×1000.

Study of astrocytic morphology by GFAP-ir and S100β-ir

In sham rats, GFAP-ir astrocytes showed a classical appearance, large and thin cellular processes in both areas. In PVL rats, in hippocampal CA1 and Cx areas, GFAP-ir astrocytes presented an enlarged cell body with more tortuous and thicker process, a hypertrophy that is typical of astroglial reaction. The morphometric analysis revealed that the astroglial cell area was increased in a 40.5% and in a 15.7% in cell number in the MHE group in hippocampal CA1 area as compared with the sham group ($p < 0.0001$). However, there were no significant differences in cell area or cell number in the Cx area when both groups were compared (Fig. 2).

Intracellular S100β-ir was observed only in astroglial cells of both analyzed brain regions. S100β protein immunostaining labeled the cell body and some of the primary cytoplasmic projections of astrocytes. In astrocytes of sham rats, S100β protein had a cytosolic localization limited to the cellular body and the primary or main cytoplasmic processes. In the PVL rats, S100β-ir had the same distribution pattern, but the intensity of the intracellular immunostaining was significantly increased in both areas. The morphometric study demonstrated that this increase was 24.3% higher in hippocampal CA1 area and 24.4% higher in brain Cx area as compared with the sham group ($p < 0.0001$) (Fig. 3).

Study of neuronal cells by NeuN-ir, MAP-2-ir, and Nf-200-ir

Neuronal cell number, counted as NeuN positive cells, was not significantly different in PVL rats in the hippocampal CA1 area or in Cx area as compared with the sham group (Fig. 4).

MAP-2-ir rendered a filament, or fiber like, immunolabeling corresponding to the neuronal dendritic process. The immunolabeled processes were observed as round stains or longitudinal tracts, according to whether dendrites were transversally or tangentially sectioned. The morphometric analysis revealed that the dendritic arborisation was decreased in 11.1% ($p < 0.01$) in the MHE group in hippocampal CA1 and in a 31.1% ($p < 0.0001$) in the Cx area as compared with the sham group (Fig. 5).

As in case of MAP-2-ir, Nf-200-ir also rendered a filament or fiber like immunolabeling, but in this case corresponding to the neuronal body, axon and dendritic process. The immunolabeled processes were observed as round stains or longitudinal tracts, according to whether the fibers were transversally or tangentially sectioned. The morphometric analysis revealed that the relative fiber area was decreased in a 19.2% ($p < 0.05$) in the MHE group in hippocampal CA1 and in a 24.1% ($p < 0.05$) in the Cx area as compared with the sham group (Fig. 6).

From a morphological point of view, some apical dendrites of the pyramidal neurons of the PVL rats showed a clear waving shape. In the sections immunostained for MAP-2 and Nf-200, the PVL animals showed fibers (corresponding both to axons and dendrites) with a clear

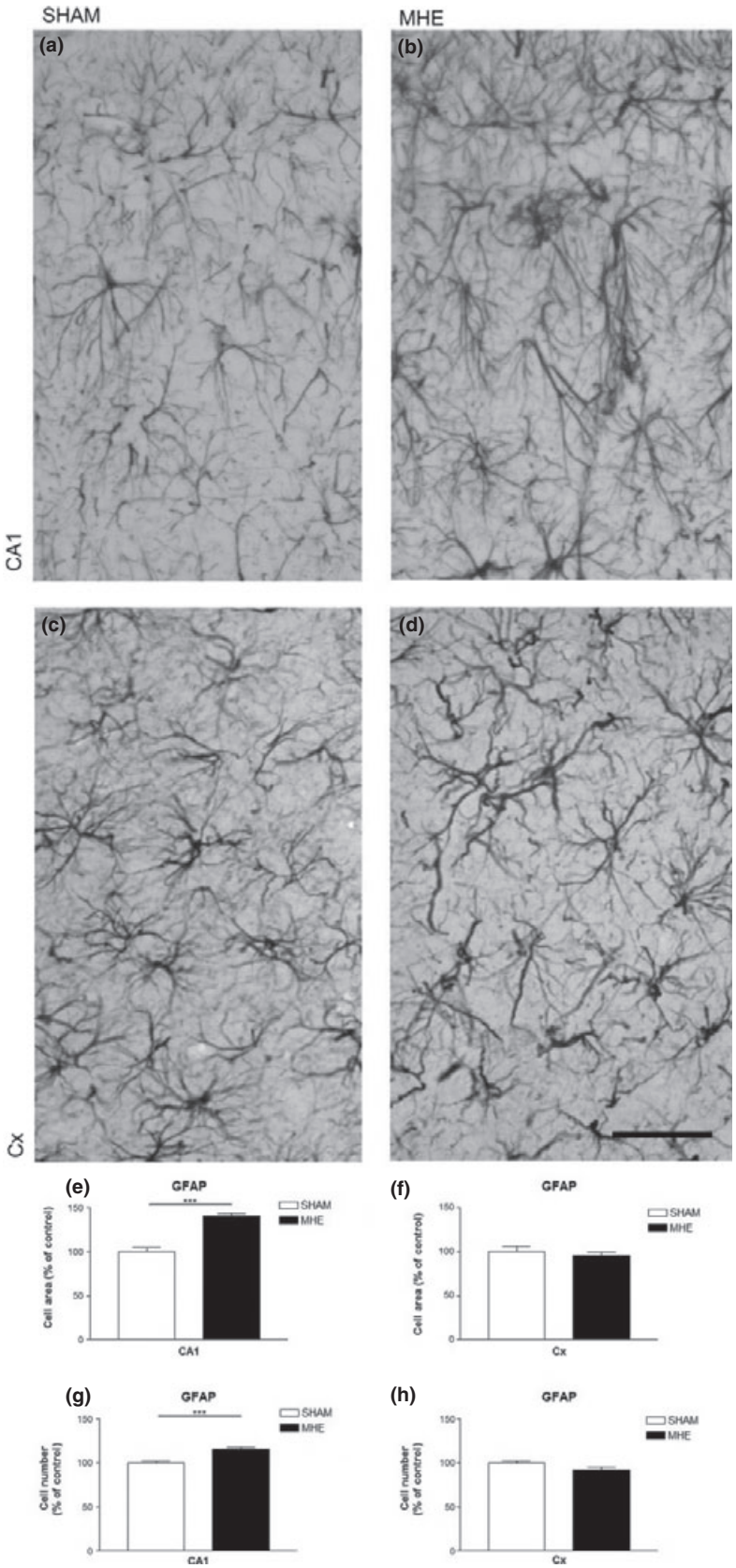

Fig. 2 Glial fibrillary acidic protein (GFAP)-ir astrocytes of the hippocampal CA1 (a and b) and brain Cx (c and d) areas of Sham (a and c) and minimal hepatic encephalopathy (MHE) (b and d) animals. Scale bar = 50 μm. Cell area (e and f) and cell number (g and h) of GFAP-ir astrocytes of the hippocampal CA1 (e and g) and brain Cx (f and h) areas of Sham and MHE animals. Values of the MHE group are represented in relation to their respective controls = 100%. ***$p < 0.0001$. Bars represent mean ± SEM.

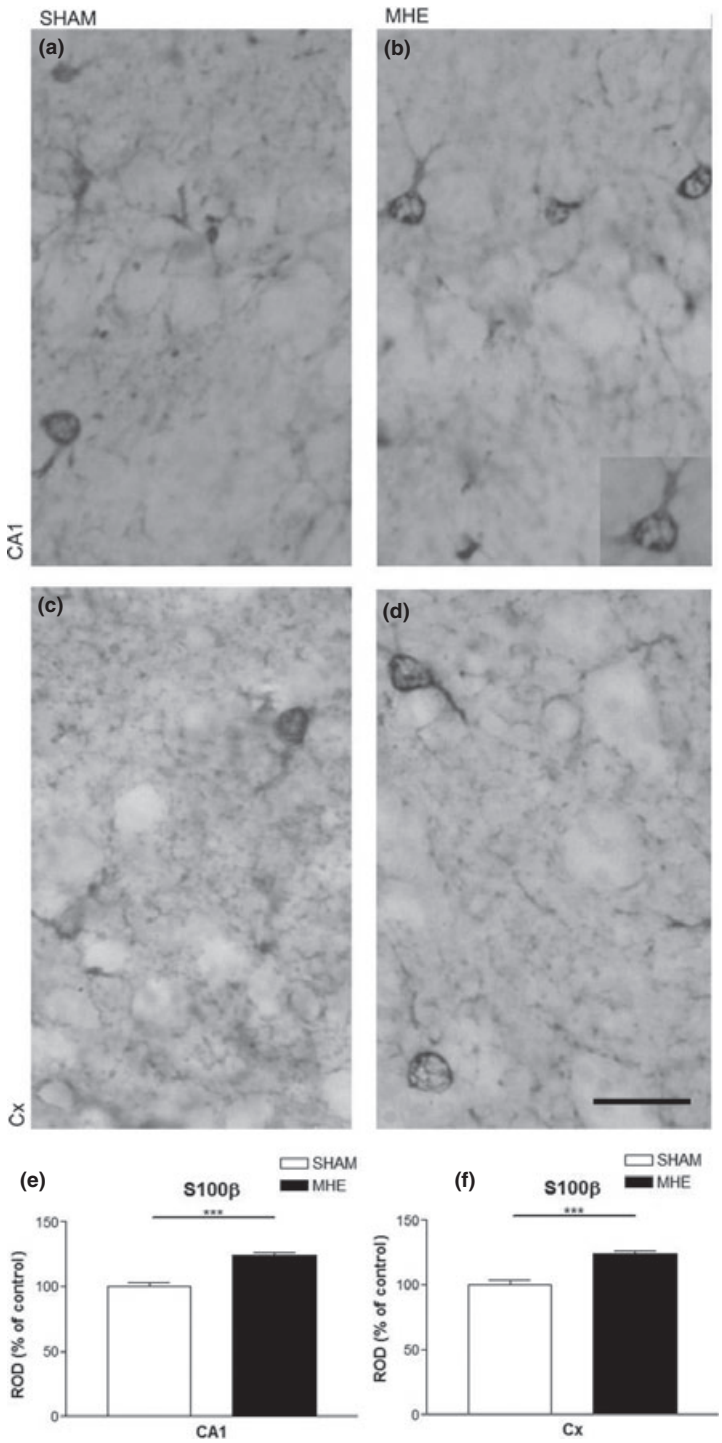

Fig. 3 S100β-ir astrocytes of the hippocampal CA1 (a and b) and brain Cx (c and d) areas of Sham (a and c) and minimal hepatic encephalopathy (MHE) (b and d) animals. Scale bar = 25 μm. Cytoplasmic relative optical density of S100β-ir astrocytes of the hippocampal CA1 (e) and brain Cx (f) areas of Sham and MHE animals. Values of the MHE group are represented in relation to their respective controls = 100%. ***$p < 0.0001$. Bars represent mean ± SEM.

waving and zigzagging shape in the Cx area. This morphological change was observed in particular in the cortical layer V, but not in the other layers of the cortex. The pyramidal neurons of the PVL animals, compared with the sham group, showed waving shape dendrites that, taking into account that the section thickness was of 50 μm and it probably included the whole thickness of the main dendrites, might be described as a corkscrew-like structure. The apical dendrites seemed to be the most affected type of dendrites in the pyramidal neurons of the MHE group. However, this structural alteration could be also observed in the basal dendrites (Fig. 7).

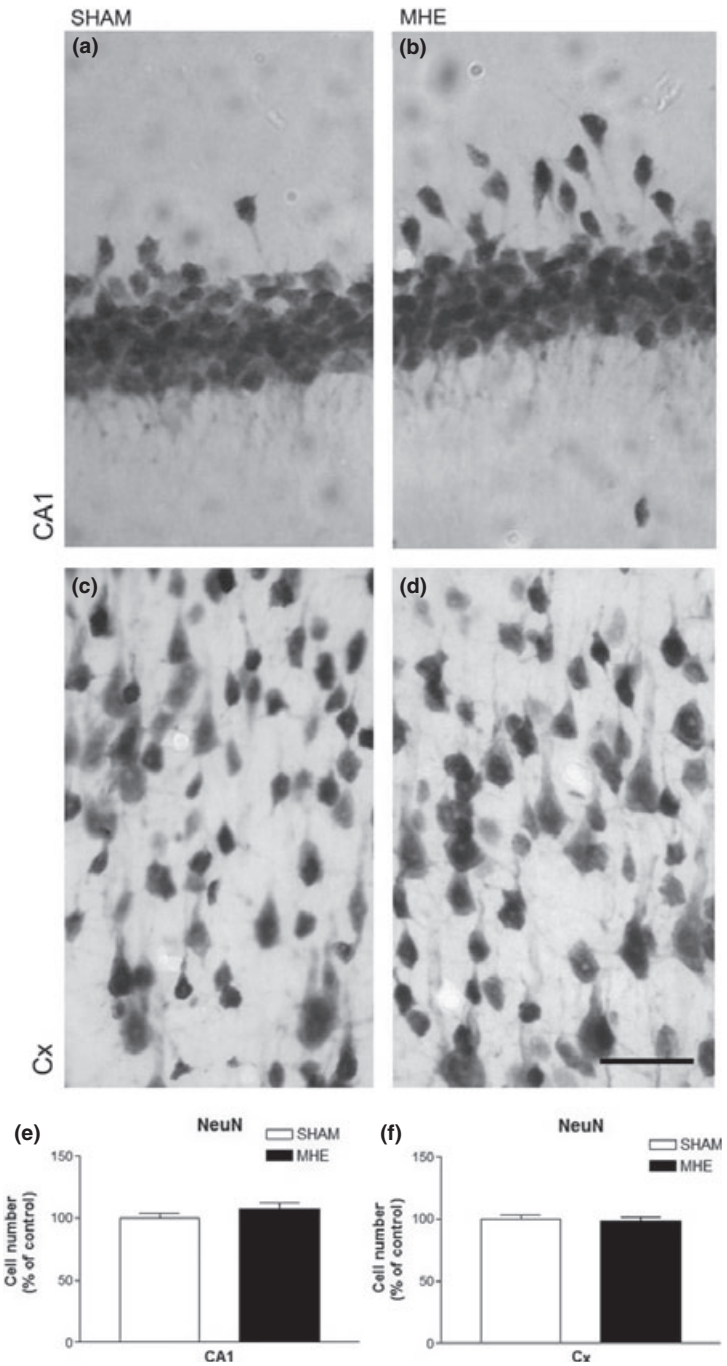

Fig. 4 Nuclear neuronal marker (NeuN)-ir neurons of the hippocampal CA1 (a and b) and brain Cx (c and d) areas of Sham (a and c) and minimal hepatic encephalopathy (MHE) (b and d) animals. Scale bar = 50 μm. Cell number of NeuN-ir neurons of the hippocampal CA1 (e) and brain Cx (f) areas of Sham and MHE animals. Values of the MHE group are represented in relation to their respective controls = 100%. Bars represent mean ± SEM.

Study of capillary vessels by Nestin-ir

Capillaries were labeled with specific antibodies against Nestin. In PVL rats, Nestin-ir presented modifications of the diameter of blood vessels showing a thicker process in both areas studied. The morphometric analysis revealed that the capillary area was increased in a 85.2% in the MHE group in hippocampal CA1 area as compared with the sham group ($p < 0.0001$). However, there were no significant differences in the capillary area in the Cx when MHE and sham groups were compared (Fig. 8).

Expression of the transcription factor HIF-1α and the downstream proteins P-gp and Epo-R

HIF-1α staining was expressed in the Cx of the PVL animals (Fig. 9a and b). To assess whether this increase corresponds to astrocytes or neurons, a double immunostaining was

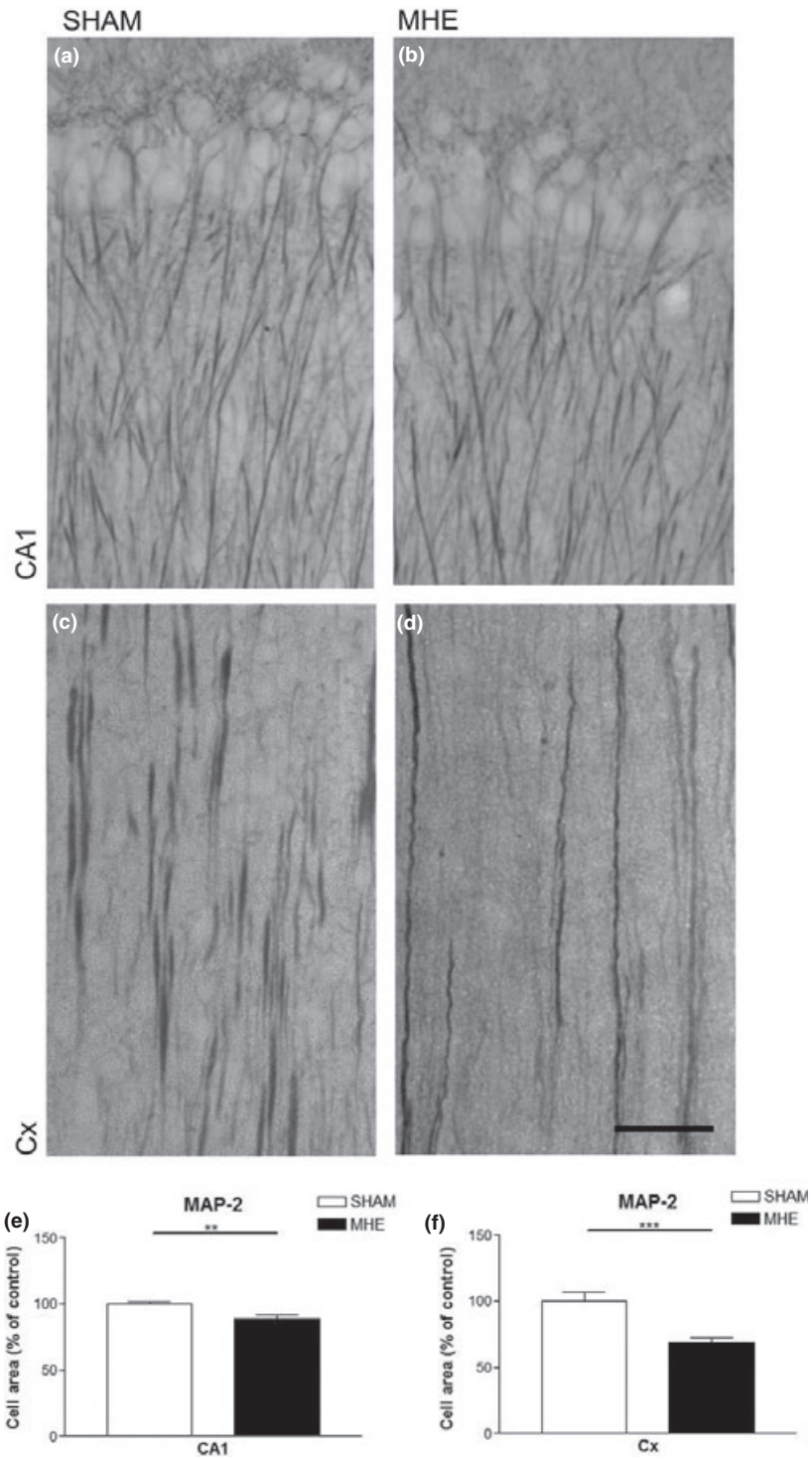

Fig. 5 Microtubule associated protein-2 (MAP-2)-ir fibers of the hippocampal CA1 (a and b) and brain Cx (c and d) areas of Sham (a and c) and minimal hepatic encephalopathy (MHE) (b and d) animals. Scale bar = 50 μm. Relative area of MAP-2-ir fibers of the hippocampal CA1 (e) and brain Cx (f) areas of Sham and MHE animals. Values of the MHE group are represented in relation to their respective controls = 100%. $^{**}p < 0.01$; $^{***}p < 0.0001$. Bars represent mean ± SEM.

performed using S-100β-HIF-1α and NeuN-HIF-1α showing that the expression of the transcription factor HIF-1α occurred in cortical neurons (Fig. 9c–e).

As a control, to confirm that the HIF-1α expressed under these conditions was functional, we studied the expression of two HIF-1α target proteins, P-gp and Epo-R, in the same area. Both showed an increased label in MHE animals (Fig. 9f–i).

Arterial blood pressure and arterial blood gasometry

To assess if rats with PVL presented a hypoxemic state related with the focal hypoxic tissue state, the arterial blood pressure

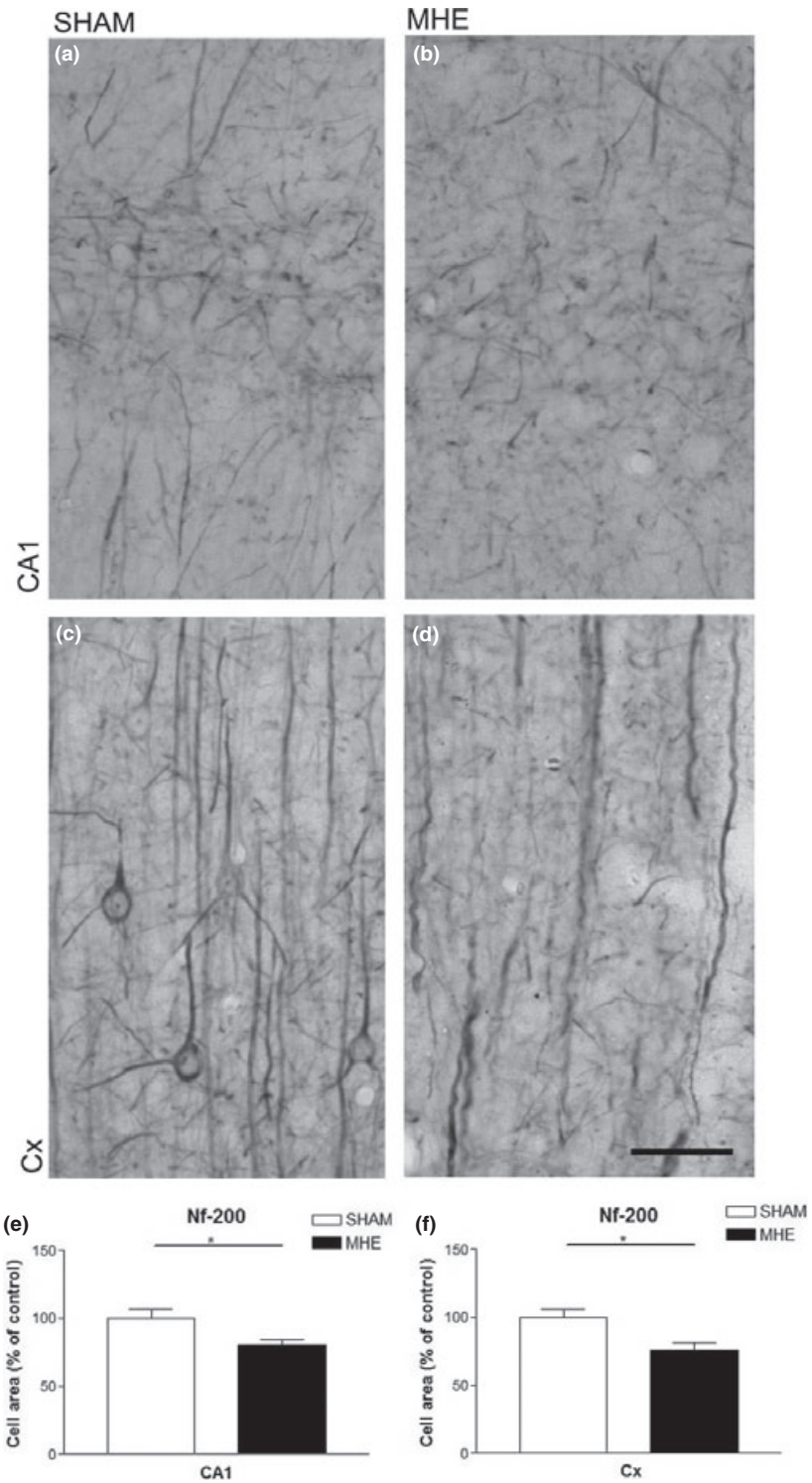

Fig. 6 Neuronal filaments 200 kDa (Nf-200)-ir fibers of the hippocampal CA1 (a and b) and brain Cx (c and d) areas of Sham (a and c) and minimal hepatic encephalopathy (MHE) (b and d) animals. Scale bar = 50 μm. Relative area of Nf-200-ir fibers of the hippocampal CA1 (e) and brain Cx (f) areas of Sham and minimal hepatic encephalopathy (MHE) animals. Values of the MHE group are represented in relation to their respective controls = 100%. $*p < 0.05$. Bars represent mean ± SEM.

and arterial blood gasometry were performed at day 10 after surgery and, to remove any concern that the changes were described because of a complication of hypoxia-ischemia, we also performed this measurements at 24 and 48 h after surgery. We found no significant differences in any of the parameters evaluated (data not shown).

Discussion

Structural and functional alterations of neural cells are described in neurons, astrocytes, and capillary endothelial cells in the brain cortex and hippocampal CA1 area. This is the first time that these findings are presented in the MHE

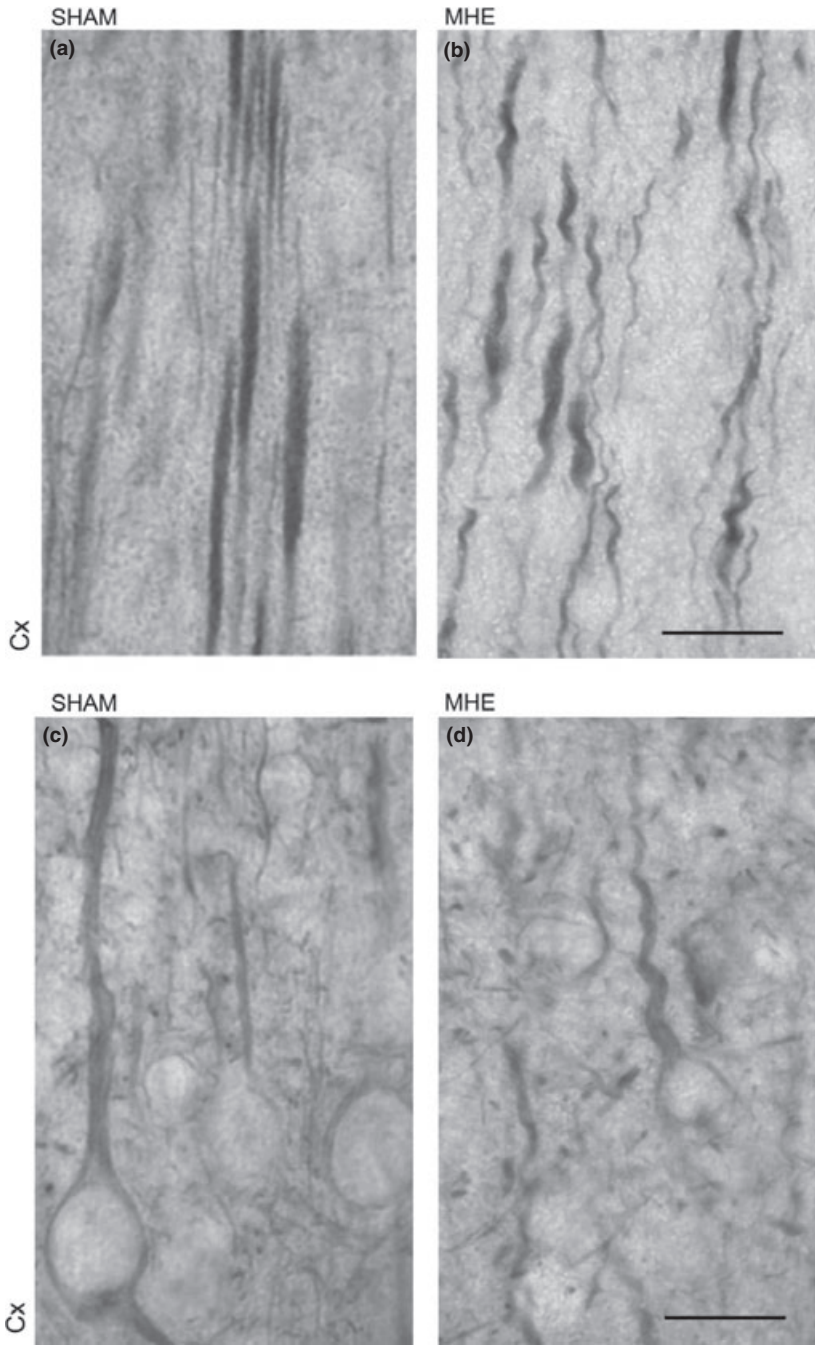

Fig. 7 Microtubule associated protein-2 (MAP-2)-ir fibers of the cortical layer V of Sham (a) and minimal hepatic encephalopathy (MHE) (b) animals. Scale bar = 25 μm. The photomicrographs show the neuronal filaments 200 kDa (Nf-200)-ir fibers of the cortical layer V of Sham (c) and MHE (d) animals. Scale bar = 25 μm.

model induced by PVL, or in any other experimental model of liver disease with portal hypertension with moderated hyperammonemia. Herein, as the cellular changes described are similar to those reported in some ischemic conditions, HIF-1α, P-gp, and Epo-R were also evaluated and focal hypoxia or a hypoxia-like state is reported.

An important histological finding in this work is the presence of Alzheimer type II astrocytes, the hallmark of HE. They were specially searched in the Cx and hippocampal areas. Brains of PVL rats were fixed by immersion, taking into account that these cells are not observed following perfusion. Alzheimer type II astrocytes were present neighboring the pyramidal layer of the hippocampus. This finding agrees with the fact that hyperammonemia is the main key factor in the PVL model of MHE.

We studied two different regions of the brain finding dissimilar results in each region; this defines that the brain is not affected homogeneously. It is difficult with the present

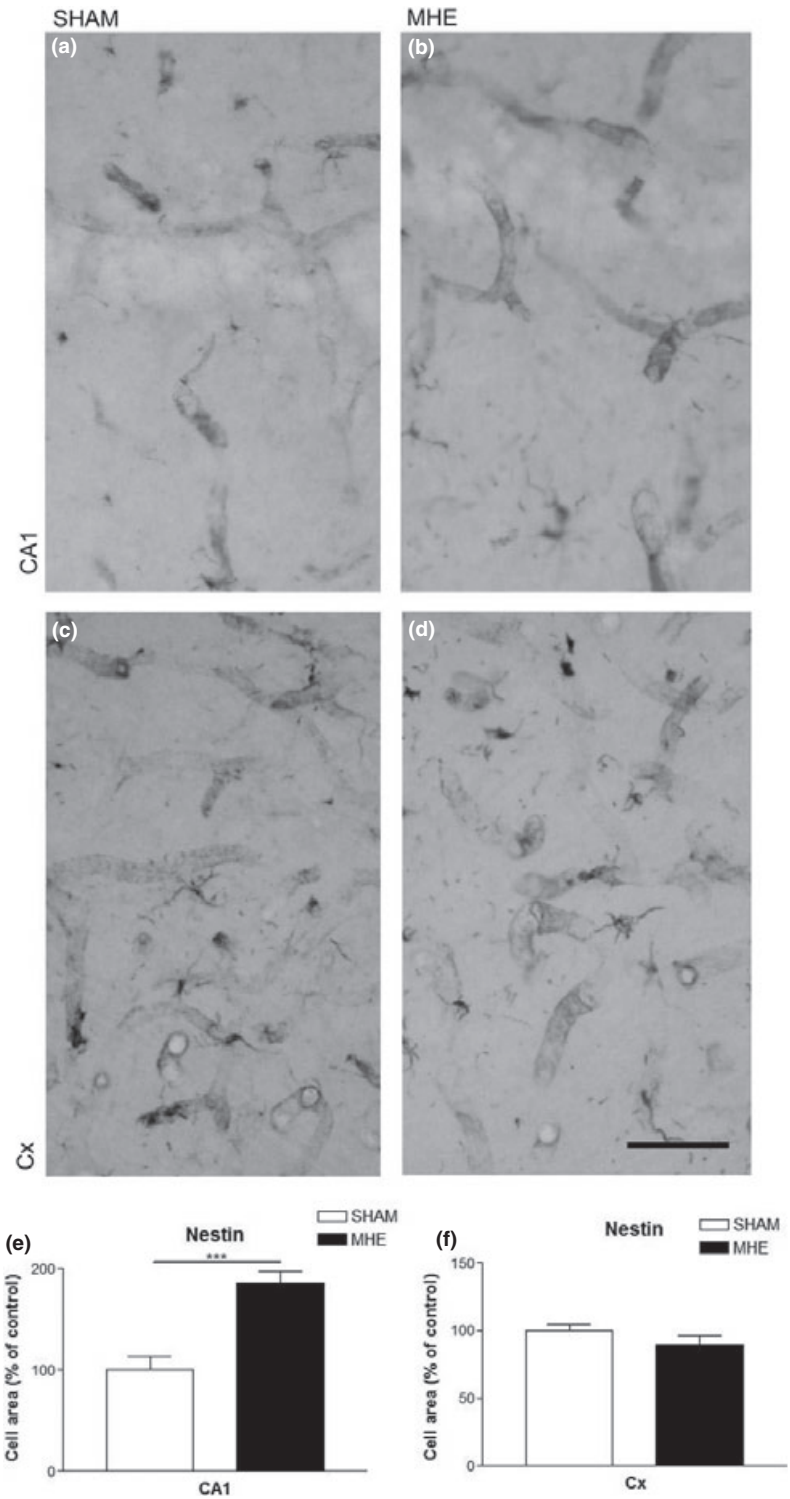

Fig. 8 Nestin-ir vessels of the hippocampal CA1 (a and b) and brain Cx (c and d) areas of Sham (a and c) and minimal hepatic encephalopathy (MHE) (b and d) animals. Scale bar = 50 μm. Capillary area of Nestin-ir vessels of the hippocampal CA1 (e) and brain Cx (f) areas of Sham and MHE animals. Values of the MHE group are represented in relation to their respective controls = 100%. ***$p < 0.0001$. Bars represent mean ± SEM.

results to suggest a conclusive pathway for this. Although these changes are in accordance with the cerebral blood flow redistribution and the increased glucose utilization of the basal ganglia, the hippocampus, and the cerebellum, described in early stages of HE (Weissenborn *et al.* 2004).

The MHE group showed in the morphometric analysis of GFAP-ir, a sensitive parameter to evaluate the astroglial response (Evrard *et al.* 2006), a significant increased expression in hippocampal CA1 region. The cell bodies were enlarged and the cytoplasmic processes were thicker,

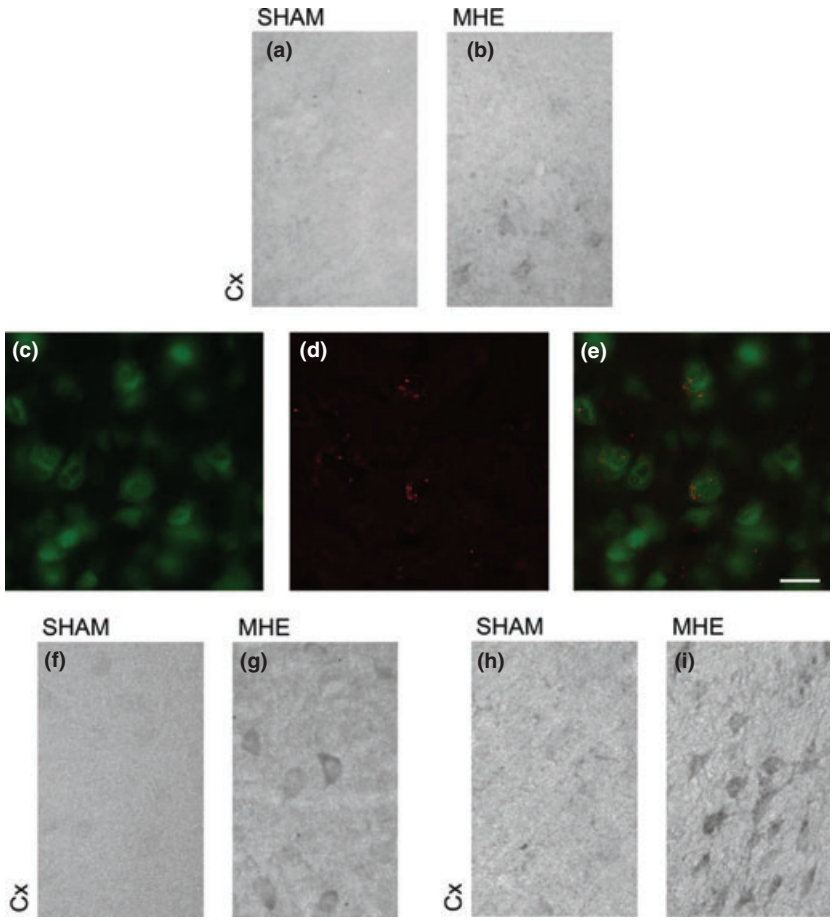

Fig. 9 Hypoxia-inducible factor 1α (HIF 1α) immunostaining in brain Cx showing the increased staining of this transcription factor in minimal hepatic encephalopathy (MHE) (b) animals compared with the Sham group (a). Scale bar = 50 μm. Double immunostaining showing HIF-1α and nuclear neuronal marker (NeuN) co-expression in the brain Cx (e) indicating that HIF-1α abundance was increased in NeuN positive neurons in MHE group. NeuN is labeled with green (c) while HIF-1α is labeled with red (d). Scale bar = 50 μm. P-gp immunostaining in brain Cx showing the increased label in MHE (g) animals compared with the Sham group (f). Scale bar = 50 μm. Erythropoietin receptor (Epo-R) immunostaining in brain Cx showing the increased label in MHE (i) animals compared with the Sham group (h). Scale bar = 50 μm.

more tortuous, and ramified. Thus, PVL produced an astroglial response in this brain area. It is well known that after several types of brain injuries caused by alcohol, cocaine, cannabinoid, electrical shock, concussions, etc., astrocytes became reactive increasing the expression of GFAP and the resulting morphological changes (Brusco *et al.* 1997; Ridet *et al.* 1997; Tagliaferro *et al.* 2002; Otani *et al.* 2006). However, GFAP did not displayed significant changes in the Cx.

The S100β protein is a dimeric astroglial cytosolic member of the S100β calcium (Ca^{2+})-binding proteins (Whitaker-Azmitia *et al.* 1997; Azmitia 2001; Donato 2003). Once released, the S-100β protein may act on neurons by entering them, binding Ca^{2+} and forming a tetrameric structure that directly binds with some cytoskeletal proteins (such as MAP-2, Nf- 200, and others) or inhibits their phosphorylation by inhibiting protein kinase C. In both cases, it stabilizes the neuronal cytoskeletal structure. This stabilization promotes neurite outgrowth, the establishment of new neural circuits and the maintenance of the existing ones which, in turn, allows the establishment of new neural synaptic contacts that will eventually allow the acquisition of cognitive and behavioral skills (Azmitia 2001; Donato 2003). In addition, S-100β interacts with GFAP in astrocytes inducing its expression and increasing branching of these glial cells (Reeves *et al.* 1994; Huttunen *et al.* 2000, 2002). The increased immunoreactivity in hippocampal astrocytes observed in the PVL rats could be related to an elevated production of S100β and/or a cytoplasmatic accumulation, because of reduced release. In the case of cortex, the increase in S100β ROD is not related with an increased in the GFAP immunoreactivity but is concomitant with reduction of neuronal process accompanied with morphological alterations in the neuronal cytoskeleton.

Glutamate plays a major role in the astrocytes–neurons interaction. Both cells work coordinately to maintain the extracellular levels of glutamate at optimal concentrations, which would otherwise be neurotoxic (Choi 1992 and Sonnewald *et al.* 2002). In the adult brain, astrocytes behave as targets of neuronal signals responding to increase concentration of glutamate, increasing intracellular Ca^{2+} concentrations that favor the phosphorylation of GFAP. Moreover, some evidence suggests that glutamate and its receptors might be involved in the reduction of MAP-2 protein expression (Sáez *et al.* 1999). Excess of glutamate, as also occurs in this MHE model (data not shown), decreases dendrite growth through a mechanism resulting from NMDA receptor activation (Monnerie *et al.* 2003). Activation of NMDA receptors, over-expressed in HE (Kosenko *et al.* 2000), increase intracellular Ca^{2+} concentration in the post-synaptic neuron, leading to the activation of various enzymes that finally leads to the proteolysis of MAP-2 and derangement of the microtubular network (Miñana *et al.* 1998 and Llansola *et al.* 1999). It was documented that ammonia exposure also leads to degradation of MAP-2 suggesting the involvement of NMDA receptors (Sáez *et al.* 1999), in agreement with the present results.

The neuronal shape and the extension of cytoplasmic processes depend on the cytoskeleton integrity. MAP-2-ir and Nf-200-ir were significantly decreased in both studied areas, suggesting a reduction of neuronal process. These neuronal changes may be associated with the increase in the intracellular astroglial S100β content.

In this study, neuronal cytoskeleton presents qualitative and structural changes. Both MAP-2-ir and Nf-200-ir fibers rendered waving-shape corkscrew-like images in the brain cortex of PVL animals (Fig. 7). Muramatsu *et al.* and Onizuka *et al.* have found shrunken soma and similar corkscrew-like apical dendrites in the pyramidal neurons of the parietal cortex in rats subjected to a hypoxic–ischemic insult (Onizuka *et al.* 1996 and Muramatsu *et al.* 1997). These cytoskeletal alterations were also seen as a common structural feature of neuronal damage in other circumstances such as neurodegenerative diseases, concussive head injury, electric shocks, prenatal ethanol exposure, perinatal asphyxia, and severe antisocial personality disorders (Evrard *et al.* 2003, 2006; Evrard and Brusco 2011).

Within the CNS, capillary blood vessels form a network highly interconnected that direct and maintain blood flow throughout the different regions. In the adult brain, the vascular supply is not homogenous and marked differences exist in the capillary density present within specific brain regions. It has been proposed that the density of the vasculature network is related to the different levels of the metabolic activity (Cavaglia *et al.* 2001). The increase of Nestin-ir in CA1 of hippocampus can be related with an altered metabolic support to neurons, thus the tissue responds with a vasculature modification. It seems that the adjustment of blood supply to increased metabolic activity occurs locally and via modifications of the capillaries area. The endothelial cells from capillaries were labeled with specific antibodies against Nestin (Alonso *et al.* 2005), an intermediate filament protein expressed by these cells, usually used as a marker of newly formed vessels. It can be assumed that new vessels are continuously added to the brain vasculature via sparse angiogenic events. Angiogenesis process represents a local tissue that also responds to decreased oxygenation.

At the molecular level, angiogenesis occur via the coordinated action of oxygen-responsive molecules such as the HIF, among others (Lee *et al.* 2009). The HIF-1α regulates the transcription of various angiogenic factors, as the vascular endothelial growth factor, and plays an important role in the vascular development (Comerford *et al.* 2002 and Wartenberg *et al.* 2003; Ke and Costa 2006). Beside this, HIF-1α induces several gene expressions as the multidrug resistance gene and its product, P-gp, related with drug refractory phenotype, as well as the erythropoietin and Epo-R related with O_2 supply. It is proposed that the expression of P-gp and the Epo-R has neuroprotective actions (Sirén and Ehrenreich 2001 and Merelli *et al.* 2011). Under normoxic conditions, specific prolyl hydroxylation within the oxygen-dependent degradation domain of HIF-1α takes place. Under hypoxic conditions, HIF-1α is stabilized and able to induce the expression of genes (Rabie and Marti 2008). The expression of HIF-1α immunostaining in the brain Cx of the MHE animals corresponds to neurons as it was demonstrate by double immunostaining.

To confirm that the HIF-1α expressed, under these experimental conditions, was a functional response, the immunostaining for P-gp and Epo-R was performed and the findings agree with HIF-1α results. It is important to highlight that, as far as we know, this is the first data that relate P-gp changes with moderate hyperammonemia and tissue hypoxia in the CNS in a MHE model induced by PVL. There is a need to co-express P-gp and Epo-R with NeuN and therefore to conclude that P-gp and Epo-R are also expressed in neurons.

It could be speculated that a new pathway could involve ammonia, mimics hypoxia by occupying the *von Hippel-Lindau* binding domain of HIF-1α and thereby preventing its degradation and causing the stabilization of HIF-1α with the concomitant multidrug resistance-1 and Epo-R over-expression. Because of the presence of Alzheimer type II astrocytes in MHE animals, we think that hyperammonemia, three fold higher, is the main key factor in this model; although other factors may play a secondary role. The neurotoxics involved in PVL, probably are closely related to the cytoskeletal alterations here observed, and they may affect the structural and functional neuronal-astrocytic relationship. These pathogenic mechanisms could be mediated by the HIF-1α stabilization resulting in a hypoxia-like state. The focal hypoxic state here described, is not accompanied with

hypoxemia, as evidenced in the arterial blood gases evaluation. There is now enough evidence that suggests whether ammonia induce these alterations showing a new pathway in experimental PVL pathogenesis.

Acknowledgements

The authors acknowledge Prof. Dr Michael Norenberg for his kind advises and comments in the experiment design and the results related to this article. Financial support was given by UBACYT 0687, PICT 01080, and UBACYT M0093. The authors state no conflict of interest.

References

Abraldes J. G., Pasarín M. and García-Pagán J. C. (2006) Animal models of portal hypertension. *World J. Gastroenterol.* **12**, 6577–6584.

Alonso G., Galibert E., Duvoid-Guillou A. and Vincent A. (2005) Hyperosmotic stimulus induces reversible angiogenesis within the hypothalamic magnocellular nuclei of the adult rat: a potential role for neuronal vascular endothelial growth factor. *BMC Neurosci.* **24**, 6;20.

Azmitia E. C. (2001) Modern views on an ancient chemical: serotonin effects on cell proliferation, maturation, and apoptosis. *Brain Res. Bull.* **56**, 413–424.

Brusco A., Saavedra J. P., García G., Tagliaferro P., Evangelista de Duffard A. M. and Duffard R. (1997) 2,4-dichlorophenoxyacetic acid through lactation induces astrogliosis in rat brain. *Mol. Chem. Neuropathol.* **30**, 175–185.

Bustamante J., Lores-Arnaiz S., Tallis S., Roselló D. M., Lago N., Lemberg A., Boveris A. and Perazzo J. C. (2011) Mitochondrial dysfunction as a mediator of hippocampal apoptosis in a model of hepatic encephalopathy. *Mol. Cell. Biochem.* **354**, 231–240.

Butterworth R. F., Norenberg M. D., Felipo V., Ferenci P., Albrecht J. and Blei A. T. (2009) Experimental models of hepatic encephalopathy: ISHEN guidelines. *Liver Int.* **29**, 783–788.

Caltana L., Merelli A., Lazarowski A. and Brusco A. (2009) Neuronal and glial alterations due to focal cortical hypoxia induced by direct cobalt chloride (CoCl2) brain injection. *Neurotox. Res.* **15**, 348–358.

Cavaglia M., Dombrowski S. M., Drazba J., Vasanji A., Bokesch P. M. and Janigro D. (2001) Regional variation in brain capillary density and vascular response to ischemia. *Brain Res.* **910**, 81–93.

Choi D. W. (1992) Excitotoxic cell death. *J. Neurobiol.* **23**, 1261–1276.

Comerford K. M., Wallace T. J., Karhausen J., Louis N. A., Montalto M. C. and Colgan S. P. (2002) Hypoxia-inducible factor-1-dependent regulation of the multidrug resistance (MDR1) gene. *Cancer Res.* **62**, 3387–3394.

Donato R. (2003) Intracellular and extracellular roles of S100 proteins. *Microsc. Res. Tech.* **60**, 540–551.

Eizayaga F., Scorticati C., Prestifilippo J. P., Romay S., Fernandez M. A., Castro J. L., Lemberg A. and Perazzo J. C. (2006) Altered blood-brain barrier permeability in rats with prehepatic portal hypertension turns to normal when portal pressure is lowered. *World J. Gastroenterol.* **12**, 1367–1372.

Evrard S. G and Brusco A. (2011) Etanol effects on the cytoeskeleton of nerve tissue cells, in *Cytoeskeleton of the Nervous System* (Nixon R. A. and Yuan A.,. Eds), pp. 697–758, **29**. Springer, New York.

Evrard S. G., Vega M. D., Ramos A. J., Tagliaferro P. and Brusco A. (2003) Altered neuron-glia interactions in a low, chronic prenatal ethanol exposure. *Brain Res. Dev. Brain Res.* **147**, 119–133.

Evrard S. G., Duhalde-Vega M., Tagliaferro P., Mirochnic S., Caltana L. R. and Brusco A. (2006) A low chronic ethanol exposure induces morphological changes in the adolescent rat brain that are not fully recovered even after a long abstinence: an immunohistochemical study. *Exp. Neurol.* **200**, 438–459.

Huttunen H. J., Kuja-Panula J., Sorci G., Agneletti A. L., Donato R. and Rauvala H. (2000) Coregulation of neurite outgrowth and cell survival by amphoterin and S100 proteins through receptor for advanced glycation end products (RAGE) activation. *J. Biol. Chem.* **22;275**, 40096–40105.

Huttunen H. J., Fages C., Kuja-Panula J., Ridley A. J. and Rauvala H. (2002) Receptor for advanced glycation end products-binding COOH-terminal motif of amphoterin inhibits invasive migration and metastasis. *Cancer Res.* **15;62**, 4805–4811.

Ke Q. and Costa M. (2006) Hypoxia-inducible factor-1 (HIF-1). *Mol. Pharmacol.* **70**, 1469–1480.

Kosenko E., Kaminsky Y., Stavroskaya I. G. and Felipo V. (2000) Alteration of mitochondrial calcium homeostasis by ammonia-induced activation of NMDA receptors in rat brain in vivo. *Brain Res.* **13;880**, 139–146.

Lee H. S., Han J., Bai H. J. and Kim K. W. (2009) Brain angiogenesis in developmental and pathological processes: regulation, molecular and cellular communication at the neurovascular interface. *FEBS J.* **276**, 4622–4635.

Llansola M., Miñana M. D., Montoliu C., Saez R., Corbalán R., Manzo L. and Felipo V. (1999) Prenatal exposure to aluminum reduces expression of neuronal nitric oxide synthase and of soluble guanylate cyclase and impairs glutamatergic neurotransmission in rat cerebellum. *J. Neurochem.* **A73**, 712–718.

Lores-Arnaiz S., Perazzo J. C., Prestifilippo J. P., Lago N., D'Amico G., Czerniczyniec A., Bustamante J., Boveris A. and Lemberg A. (2005) Hippocampal mitochondrial dysfunction with decreased mtNOS activity in prehepatic portal hypertensive rats. *Neurochem. Int.* **47**, 362–368.

Merelli A., Caltana L., Lazarowski A. and Brusco A. (2011) Experimental evidence of the potential use of erythropoietin by intranasal administration as a neuroprotective agent in cerebral hypoxia. *Drug Metabol. Drug Interact.* **26**, 65–69.

Miñana M. D., Montoliu C., Llansola M., Grisolía S. and Felipo V. (1998) Nicotine prevents glutamate-induced proteolysis of the microtubule-associated protein MAP-2 and glutamate neurotoxicity in primary cultures of cerebellar neurons. *Neuropharmacology* **37**, 847–857.

Monnerie H., Shashidhara S. and Le Roux P. D. (2003) Effect of excess extracellular glutamate on dendrite growth from cerebral cortical neurons at 3 days in vitro: Involvement of NMDA receptors. *J. Neurosci. Res.* **74**, 688–700.

Muramatsu K., Fukuda A., Togari H., Wada Y. and Nishino H. (1997) Vulnerability to cerebral hypoxic-ischemic insult in neonatal but not in adult rats is in parallel with disruption of the blood-brain barrier. *Stroke* **28**, 2281–2288.

Norenberg M. D. (1977) A light and electron microscopic study of experimental portal-systemic (ammonia) encephalopathy. Progression and reversal of the disorder. *Lab. Invest.* **36**, 618–627.

Olde Damink S. W., Jalan R., Redhead D. N. *et al.* (2002) Interorgan ammonia and amino acid metabolism in metabolically stable patients with cirrhosis and a TIPSS. *Hepatology* **36**, 1163–1171.

Onizuka K., Fukuda A., Kunimatsu M., Kumazaki M., Sasaki M., Takaku A. and Nishino H. (1996) Early cytopathic features in rat ischemia model and reconstruction by neural graft. *Exp. Neurol.* **137**, 324–332.

Otani N., Nawashiro H., Fukui S., Ooigawa H., Ohsumi A., Toyooka T., Shima K., Gomi H. and Brenner M. (2006) Enhanced hippocampal neurodegeneration after traumatic or kainate excitotoxicity in GFAP-null mice. *J. Clin. Neurosci.* **13**, 934–938.

Rabie T. and Marti H. (2008) Brain protection by erythropoietin: a manifold task. *Physiology* **23**, 263–274.

Ramos A. J., Tagliaferro P., López E. M., Pecci Saavedra J. and Brusco A. (2000) Neuroglial interactions in a model of para-chlorophenylalanine-induced serotonin depletion. *Brain Res.* **883**, 1–14.

Reeves R. H., Yao J., Crowley M. R., Buck S., Zhang X., Yarowsky P., Gearhart J. D. and Hilt D. C. (1994) Astrocytosis and axonal proliferation in the hippocampus of S100β transgenic mice. *Proc. Natl Acad. Sci. USA* **91**, 5359–5363.

Ridet J. L., Malhotra S. K., Privat A. and Gage F. H. (1997) Reactive astrocytes: cellular and molecular cues to biological function. *Trends Neurosci.* **20**, 570–577.

Sáez R., Llansola M. and Felipo V. (1999) Chronic exposure to ammonia alters pathways modulating phosphorylation of microtubule-associated protein 2 in cerebellar neurons in culture. *J. Neurochem.* **73**, 2555–2562.

Sirén A. L. and Ehrenreich H. (2001) Erythropoietin–a novel concept for neuroprotection. *Eur. Arch. Psychiatry Clin. Neurosci.* **251**, 179–184.

Sonnewald U., Qu H. and Aschner M. (2002) Pharmacology and toxicology of astrocyte-neuron glutamate transport and cycling. *J. Pharmacol. Exp. Ther.* **301**, 1–6.

Tagliaferro P., Vega M. D., Evrard S. G., Ramos A. J. and Brusco A. (2002) Alcohol exposure during adulthood induces neuronal and astroglial alterations in the hippocampal CA-1 area. *Ann. N. Y. Acad. Sci.* **965**, 334–342.

Vorobioff J., Bredfeldt J. E. and Groszmann R. J. (1983) Hyperdynamic circulation in portal-hypertensive rat model: a primary factor for maintenance of chronic portal hypertension. *Am. J. Physiol.* **244**, G52–G57.

Wartenberg M., Ling F. C., Müschen M., Klein F., Acker H., Gassmann M., Petrat K., Pütz V., Hescheler J. and Sauer H. (2003) Regulation of the multidrug resistance transporter P-glycoprotein in multicellular tumor spheroids by hypoxia-inducible factor (HIF-1) and reactive oxygen species. *FASEB J.* **17**, 503–505.

Weissenborn K., Bokemeyer M., Ahl B., Fischer-Wasels D., Giewekemeyer K., van den Hoff J., Köstler H. and Berding G. (2004) Functional imaging of the brain in patients with liver cirrhosis. *Metab. Brain Dis.* **19**, 269–280.

Whitaker-Azmitia P. M., Wingate M., Borella A., Gerlai R., Roder J. and Azmitia E. C. (1997) Transgenic mice overexpressing the neurotrophic factor S-100 beta show neuronal cytoskeletal and behavioral signs of altered aging processes: implications for Alzheimer's disease and Down's syndrome. *Brain Res.* **776**, 51–60.